Supplementary Information

One-Pot Synthesis for Doping and Coating NMC 811 with B, Al, and Nb for Enhanced Stability

*Rex Chen[1], Vahid Moradi[2], Lida Hadidi[2], and Byron D. Gates[1] **

[1]Department of Chemistry, Simon Fraser University, 8888 University Drive, Burnaby, BC V5A 1S6 (Canada)

[2]Nano One Materials Corporation, 8575 Government St., Burnaby, BC, V3N 4V1 (Canada)

* Corresponding Author: bgates@sfu.ca

This research was conducted in collaboration with Nano One Materials Corp. supported in part by MITACS (Reference No. R832743), the Natural Sciences and Engineering Research Council of Canada (NSERC; Grant No. RGPIN-2020-06522), and a Simon Fraser University Graduate Fellowship (R. Chen). This work used 4D LABS at Simon Fraser University (SFU) and the Center for Soft Materials shared facilities, supported by the Canada Foundation for Innovation (CFI), British Columbia Knowledge Development Fund (BCKDF), Western Economic Diversification Canada, and SFU. This work also utilized the nanoFAB at the University of Alberta to obtain the XPS measurements.

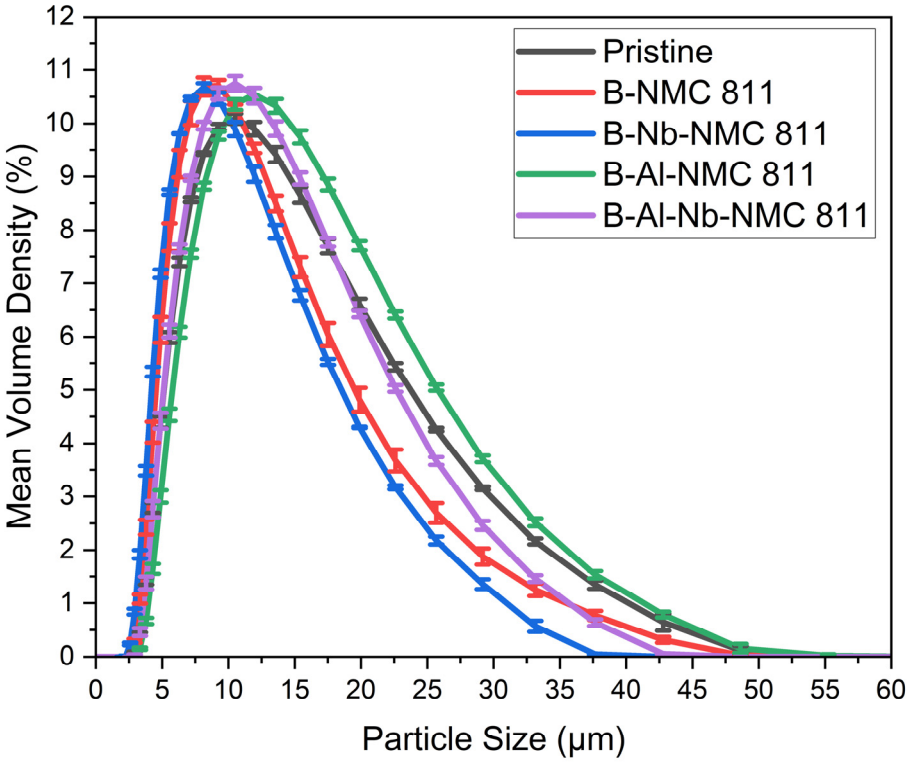

Figure S1. Particle size distribution (PSD) profiles for pristine and doped NMC 811 ($LiNi_{0.8}Mn_{0.1}Co_{0.1}O_2$) materials, showing the mean volume density as a function of secondary particle size. Each measured mean volume density is the average of five separate measurements, with error bars representing one standard deviation.

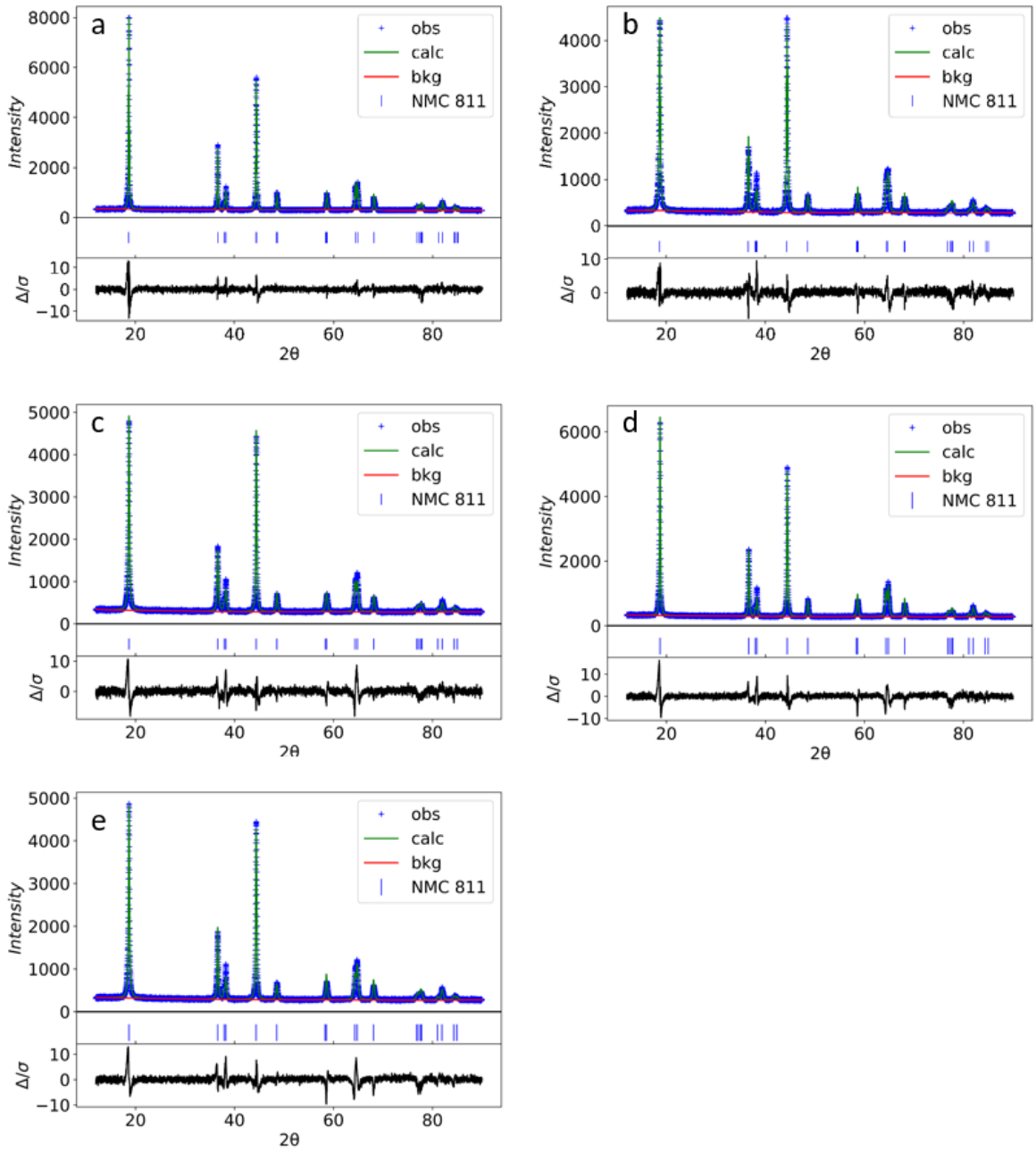

Figure S2. Plots of the Rietveld refinements generated using GSAS-II for (a) pristine NMC 811, (b) B-NMC 811, (c) B-Al-NMC 811, (d) B-Nb-NMC 811, and (e) B-Al-Nb-NMC 811. The observed X-ray diffraction (XRD) patterns (blue dots) are shown with the calculated profiles (green trace) from the layered $R\bar{3}m$ structural model. The difference trace (black) between the measured and calculated pattern is shown below each plot.

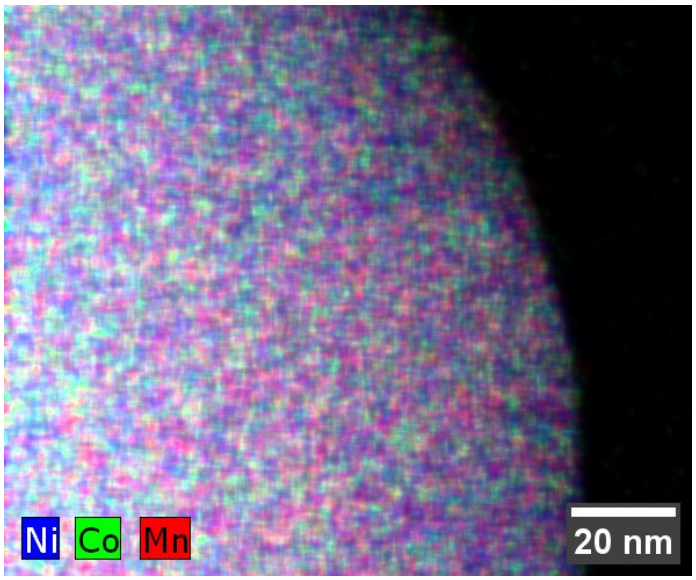

Figure S3. A representative image obtained by scanning transmission electron microscopy (STEM) combined with elemental mapping by energy-dispersive X-ray spectroscopy (EDS) techniques, which depicts the distribution of transition metals in the pristine NMC 811 sample.

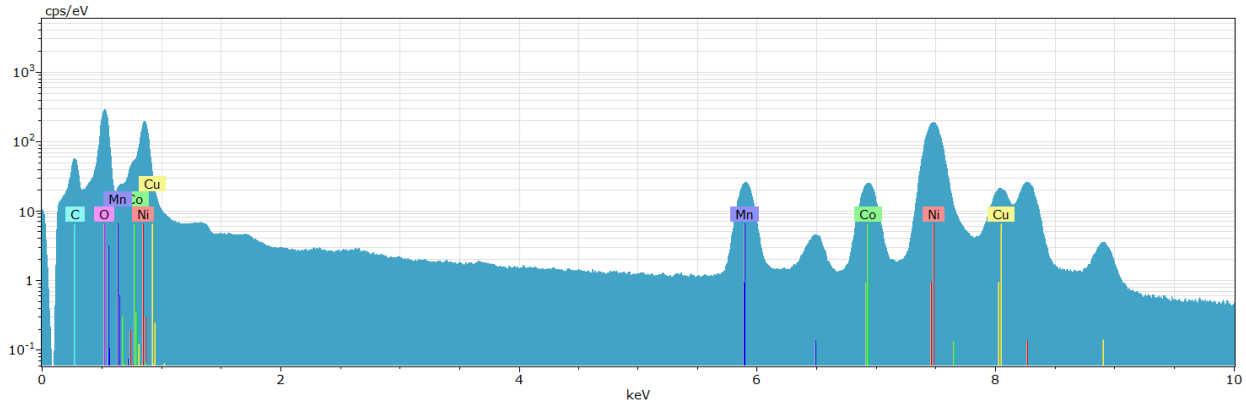

Figure S4. A representative EDS spectrum of pristine NMC 811, plotted with the y-axis on a logarithmic scale to assist in viewing all the measured peaks. The characteristic X-ray emission peaks confirm the elemental composition of $LiNi_{0.8}Mn_{0.1}Co_{0.1}O_2$. The signals from carbon and copper are contributions from the TEM grid.

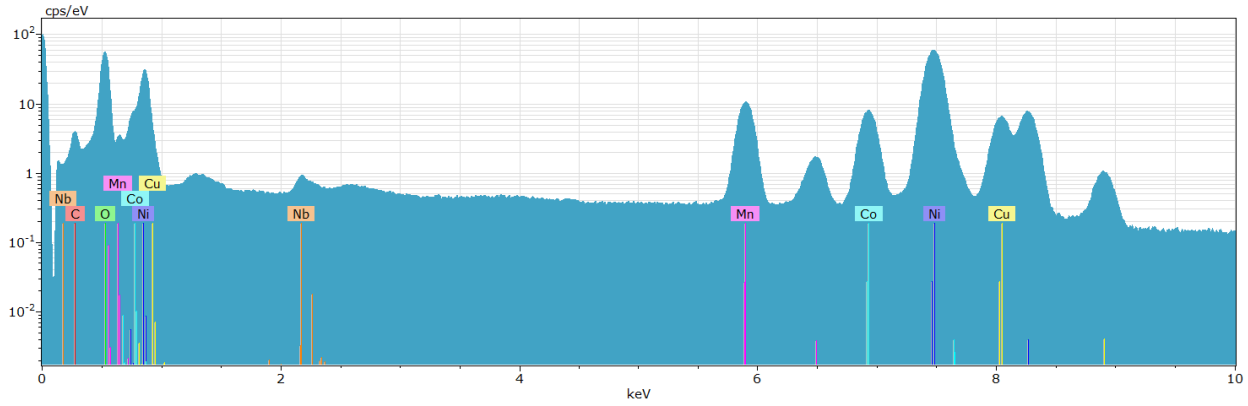

Figure S5. A representative EDS spectrum of B-Nb-NMC 811, plotted with the y-axis on a logarithmic scale to assist in viewing all the measured peaks. The characteristic X-ray emission peaks confirm the elemental composition of the $LiNi_{0.8}Mn_{0.1}Co_{0.1}O_2$, including the presence of niobium (Nb) in this modified sample. Carbon and copper signals are due to contributions from the TEM grid.

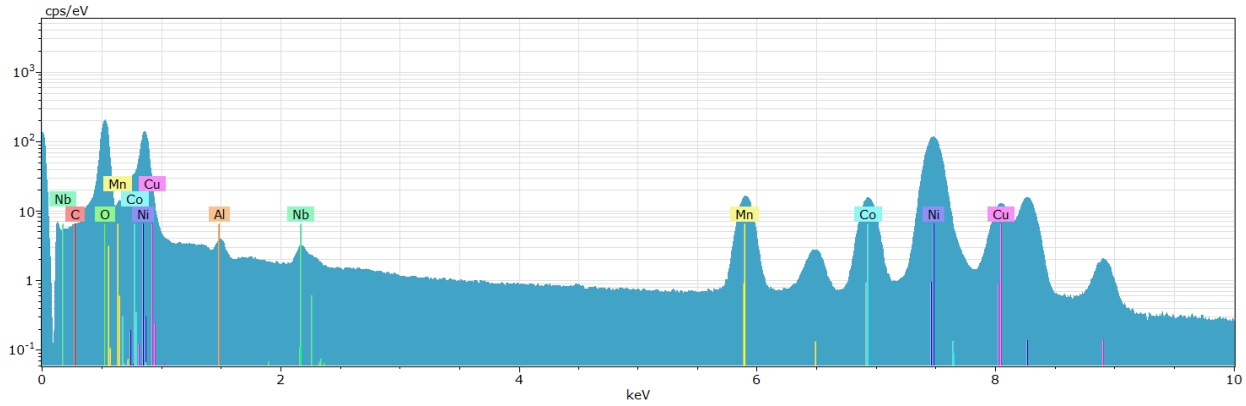

Figure S6. A representative EDS spectrum of B-Al-Nb-NMC 811, plotted with the y-axis on a logarithmic scale to assist in viewing all the measured peaks. The characteristic X-ray emission peaks confirm the elemental composition of the $LiNi_{0.8}Mn_{0.1}Co_{0.1}O_2$, including the presence of aluminum (Al) and Nb in the modified sample. The carbon and copper signals are due to contributions from the TEM grid.

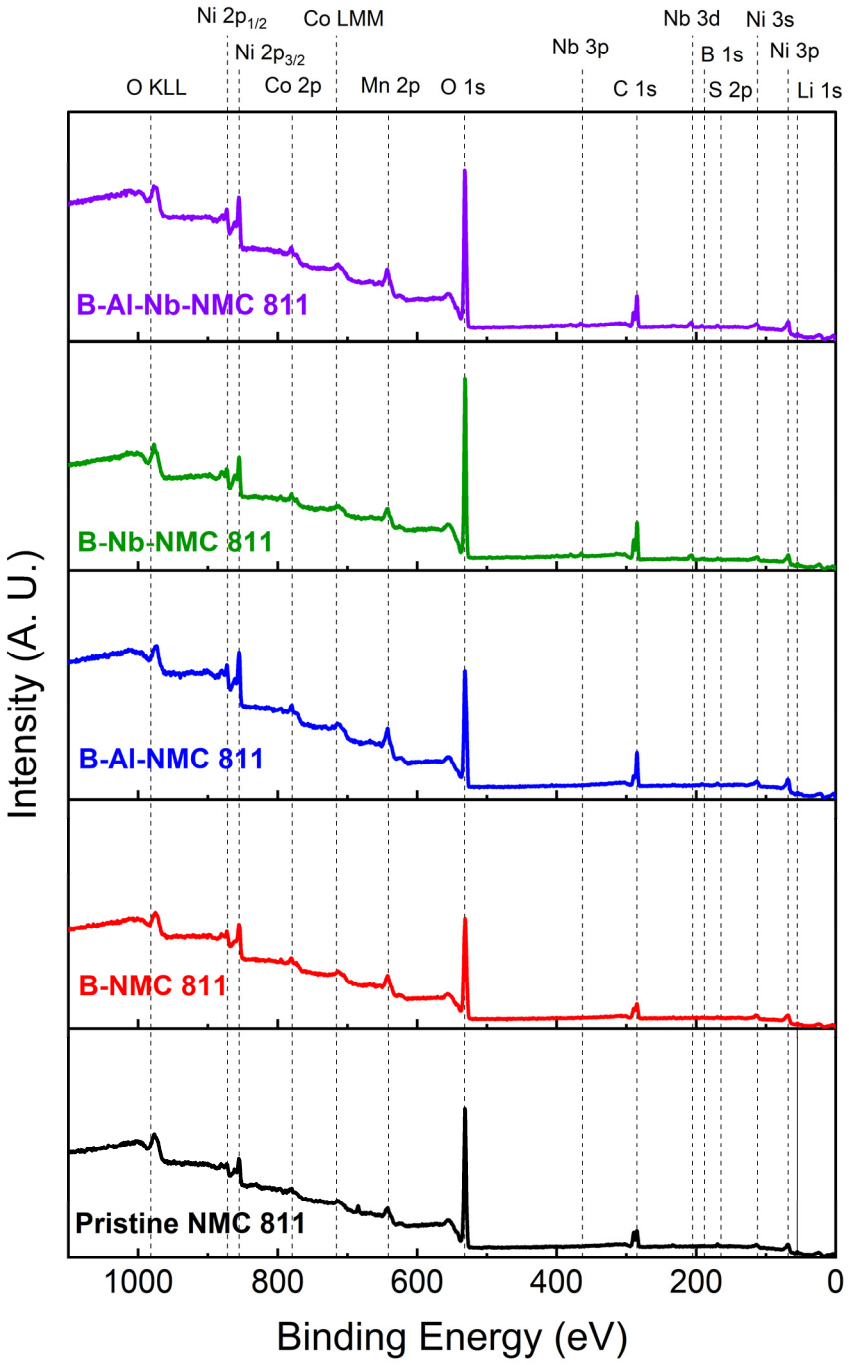

Figure S7. X-ray photoelectron spectroscopy (XPS) spectra of pristine NMC 811 and four types of modified samples. The spectra confirm the presence of the main components of NMC 811 (Li, Ni, Mn, Co, O) present on the surfaces of these materials. The successful incorporation of coating elements is verified by the appearance of B 1s and Nb 3d peaks in the relevant modified samples. Additionally, a small S 2p peak is detected in some samples, indicating the minor presence of sulfur containing impurities likely introduced during sample handling and/or transport.

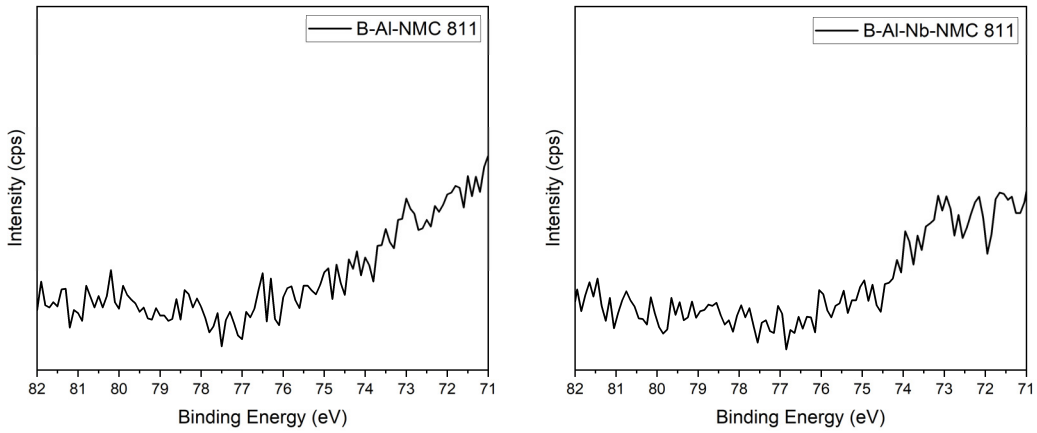

Figure S8. High-resolution X-ray photoelectron spectroscopy (XPS) spectra of the Al 2p region for the synthesized B-Al-NMC 811 and B-Al-Nb-NMC 811 samples. The absence of a distinct Al 2p peak above the baseline noise indicates that the surface concentration of aluminum is below the detection limit of the instrument.

Table S1. Elemental composition of the pristine and doped NMC 811 cathode materials before calcination as determined by inductively coupled plasma-optical emission spectrometry (ICP-OES). The values represent the normalized stoichiometric ratios of the constituent elements.

material	Li	Ni	Mn	Co	B*	Al	Nb
pristine NMC 811	1.1	0.80	0.10	0.10	0.0	0.0	0.0
B-NMC 811	1.0	0.80	0.10	0.10	0.0091	0.0	0.0
B-Al-NMC 811	1.0	0.7967	0.0967	0.0967	0.0086	0.0098	0.0
B-Nb-NMC 811	1.1	0.7984	0.0984	0.0984	0.0080	0.0	0.0047
B-Al-Nb-NMC 811	1.0	0.7946	0.0946	0.0946	0.0089	0.0098	0.0063

*Boron is assumed to occupy the interstitial sites within the crystal lattice, while aluminum and niobium occupy the octahedral sites of the transition metals.

Table S2. Elemental composition of the pristine and doped NMC 811 cathode active materials after calcination as determined by ICP-OES. The values represent the normalized stoichiometric ratios of the constituent elements.

material	Li	Ni	Mn	Co	B*	Al	Nb
pristine NMC 811	1.0	0.80	0.10	0.10	0.0	0.0	0.0
B-NMC 811	1.0	0.80	0.10	0.10	0.0088	0.0	0.0
B-Al-NMC 811	1.0	0.7967	0.0967	0.0967	0.0084	0.010	0.0
B-Nb-NMC 811	1.0	0.7985	0.0985	0.0985	0.0077	0.0	0.0046
B-Al-Nb-NMC 811	1.0	0.7949	0.0949	0.0949	0.0088	0.0098	0.0055

*Boron is assumed to occupy the interstitial sites within the crystal lattice, while aluminum and niobium occupy the octahedral sites of the transition metals.

Table S3. Summary of particle size distribution (PSD) data corresponding to the D10, D50, and D90 parameters, which represent the particle diameters at which 10%, 50%, and 90% of the sample's particles are smaller by volume, respectively, for pristine and multi-element doped NMC 811 secondary particles.

material	D10 (μm)	D50 (μm)	D90 (μm)
pristine NMC 811	5.55 (±0.0467)	11.1 (±0.0654)	23.9 (±0.205)
B-NMC 811	5.00 (±0.0632)	9.52 (±0.182)	20.4 (±0.481)
B-Al-NMC 811	6.19 (±0.0567)	12.2 (±0.0743)	25.1 (±0.191)
B-Nb-NMC 811	4.61 (±0.0298)	8.81 (±0.0381)	18.5 (±0.129)
B-Al-Nb-NMC 811	5.55 (±0.0648)	10.8 (±0.0659)	21.9 (±0.111)

Table S4. Theoretical weight percentages (wt%) of dopants in the synthesized materials, calculated based on a total material mass of 1 g and assuming 1 mol% B, 1 mol% Al, and 0.5 mol% Nb relative to 1 mol of total transition metals.

material	B wt%	Al wt%	Nb wt%
B-NMC 811	0.1110	n/a	n/a
B-Al-NMC 811	0.1107	0.2763	n/a
B-Nb-NMC 811	0.1105	n/a	0.4747
B-Al-Nb-NMC 811	0.1102	0.2750	0.4734

Table S5. Theoretical atomic percentages (at%) of dopants in the synthesized materials, calculated based on a total material mass of 1 g and assuming 1 mol% B, 1 mol% Al, and 0.5 mol% Nb relative to 1 mol of total transition metals.

material	B at%	Al at%	Nb at%
B-NMC 811	0.2494	n/a	n/a
B-Al-NMC 811	0.2488	0.2488	n/a
B-Nb-NMC 811	0.2491	n/a	0.1245
B-Al-Nb-NMC 811	0.2484	0.2484	0.1242

Table S6. Summary of pre-cycling and pre-rate capability as determined from the average discharge capacities of six distinct cells prepared for each type of NMC material.

material	1st C/10 discharge capacity (mAh/g)	2nd C/20 discharge capacity (mAh/g)	3rd C/20 discharge capacity (mAh/g)
pristine NMC 811	205.1±1.8	200.9±1.2	200.6±1.0
B-NMC 811	189.9±9.6	191.1±3.7	192.8±1.4
B-Al-NMC 811	204.7±4.9	203.2±1.6	203.2±1.3
B-Nb-NMC 811	205.0±3.4	200.7±1.5	200.9±0.8
B-Al-Nb-NMC 811	205.3±0.8	202.1±0.8	201.7±0.8